Journal of Luminescence 187 (2017) 240–246

Contents lists available at ScienceDirect

Journal of Luminescence

journal homepage: www.elsevier.com/locate/jlumin

Development of novel upconversion luminescent nanoparticle of Ytterbium/Thulium–doped beta tricalcium phosphate

Flávia R.O. Silva [a,*], Nelson B. Lima [a], Walter K. Yoshito [a], Ana Helena A. Bressiani [a], Laércio Gomes [b]

[a] Centro de Ciência e Tecnologia dos Materiais, Instituto de Pesquisas Energéticas e Nucleares, IPEN-CNEN/SP, Butantã, São Paulo SP, Brazil
[b] Centro de Lasers e Aplicações, Instituto de Pesquisas Energéticas e Nucleares, Brazil

ARTICLE INFO

Article history:
Received 11 November 2016
Received in revised form
6 March 2017
Accepted 13 March 2017
Available online 18 March 2017

Keywords:
Beta-tricalcium phosphate
Ytterbium
Thulium
Upconversion luminescence
Visible and near-infrared emitting materials
Nanoparticle

ABSTRACT

A novel class of upconversion luminescent nanocrystals of Yb/Tm:calcium deficient hydroxyapatite were synthesized by co-precipitation method in aqueous solution (pH adjusted to 6) and specially heat-treated with microwave radiation at different temperatures (from 900 °C to 1000 °C) and times (2–10 min) to produce small nanocrystals of Yb/Tm:β-tricalcium phosphate (β-TCP). As a result, we report for the first time, a single-phase Yb/Tm-doped β-TCP nanocrystals with a mean crystallite size of 55.3 nm. This material has an efficient visible luminescence from the $^1G_4$ (blue emission) and $^3F_2$ (red emission) and near infrared emission from the $^3H_4$ excited states of Tm^{3+} induced by the $Yb^{3+} \rightarrow Tm^{3+}$ energy transfer under laser excitation (Yb^{3+}) at 972 nm. This β-TCP activated by Yb^{3+} and Tm^{3+} ions constitutes a new nano-fluoroprobe that can be used as optical contrast agents, affording high resolution and sensitivity for visible-near infrared applications.

1. Introduction

Many efforts have been made to conciliate both therapy and diagnoses strategies in just an all-in-one particle, leading to advantages over single approaches [1]. Optical imaging approaches are promising high-resolution modalities for the early cancer detection and treatment, since it is a sensitive, non-invasive and real-time monitoring technique [2]. Despite all benefits, optical technique however relies upon the use of sensitive and stable probes [2].

Ongoing discoveries of potential probe molecules for photodiagnosis and phototherapy are focused on the development of imaging optical sensitivity contrast agents in the near-infrared spectrum (NIR, typically in the 700–1300 nm spectral range). At the NIR spectrum window, biological tissues show very low absorption and auto fluorescence [3]. As a result, the sensitivity for NIR imaging contrast agents is greatly enhanced, affording penetration depths of an order of magnitude greater than that of visible light and low phototoxicity to normal cells and tissues [3]. Fluorescence imaging can be achieved by endogenous (porphyrins, collagens, proteins, etc) or exogenous (optical contrast agents, such polymethines, Cy5.5 and Cy7 [3,4]) molecules. However, fluorescence imaging at depths greater than a few millimeters requires NIR probes and dyes [5].

With the oncoming of the nanomedicine and nanotechnology in the past few decades, this new field has exerted great impact on the development of novel nanoparticle-based probes for in vivo cancer molecular imaging. These probes can target tumor cells either through the EPR effect (enhanced permeability and retention) or by a specific binding between the tumor cell receptors and the biomolecules-functionalized nanoparticles [3]. NIR organic dye-containing nanoparticles have overcome some of the limitations of the conventional NIR organic dyes, such as poor photostability, rapid photobleaching, low quantum yield, low detection sensitivity, high citotoxity, etc. Most of the fluorescent nanoparticles that have been successfully applied for bioimaging applications is typically a core-shell structure, where the core is composed by a fluorescent dye, protected (by the shell) from the photobleaching [3].

A new approach to deliver light into deeper tissues for PDD (photodynamic diagnosis) and PDT (photodynamic therapy) is using NIR-excitable upconversion nanoparticles (UCNPs) as an energy donor. The generation of upconversion (UC) fluorescence is a multiphoton process. UCNPs are usually lanthanide-doped nanocrystals, which emit high-energy photons under the excitation by the NIR light, and they have proven to be valuable and desirable tools for NIRF (near infrared fluorescence) techniques [6–8].

Appropriate loading of photosensitizers (PS) molecules (including silica encapsulation, non-covalently physical adsorption, and covalent conjugation via chemical linkages) to UCNPs is important to allow effective resonance energy transfer from donors to acceptors in NIR-induced PDT [9]. Recent studies have

* Corresponding author.
E-mail address: frsilva@ipen.br (F.R.O. Silva).

http://dx.doi.org/10.1016/j.jlumin.2017.03.029
0022-2313/

demonstrated a significant reduction in tumor growth of the group treated with UCNP loaded PS (mesoporous silica coated Yb:Er:$NaYF_4$, $NaGdY_4$- PEGylation loaded with Ce6 molecules) compared to control group, showing encouraging therapeutic effect upon either local injection or systemic administration of UCNP-PS nanocomplexes [9].

In addition to the application of UCNPs as energy donors, they could also be used to trigger release or 'uncaging' of functional biomolecules. Photo-responsive drug release systems have received significant interests, since they can remotely control the releasing of therapeutic drugs at the targeting site [9]. A specific class of UCNPs, usually containing Yb^{3+} and Tm^{3+} (for example Yb:Tm:$NaYF_4$) [9,10] is able to convert the NIR laser excitation into different wavelengths from UV to NIR, and could be a great promising in the designing of NIR-light photoreactions of compounds anchored to their surfaces [9]. Recently it was reported the using of NIR-to-UV UCNPs for photo-controllable gene expression [11], where the authors have used the NIR light treatment to uncaging the pDNA and siRNA by the energy transferred from the UCNPs, photo inducing controlled gene expression and specific gene silencing.

xAs summarized, these nanoprobes play an important role in early detection, screening, image-guided therapy, photodiagnosis, phototherapy, gene therapy for controlled and specific gene delivery/knockdown [9], but brighter UCNPs need to be synthesized with higher quantum yield (UNCPs quantum yields is mostly less than 1%, limiting their using in PDD and PDT [9]) and appropriate loading of PS molecules onto the UCNPs (to allow effective resonance energy transfer from donors to acceptors), by designing special UCNP structures.

In this context, nanosized calcium phosphate (CP) particles are particularly attractive because of the following advantages: 1) it is regarded as safe by the FDA (Federal Drug Administration) [12], since it is the main inorganic constituent of bone and teeth; 2) high biocompatibility and biodegradability; 3) the CP structures can be loaded with multiple therapeutics agents to offer synergistic effects, as photosensitizers, drugs or genes; 4) CP can be coated with biocompatible polymers that render them water-soluble in order to manage the blood circulation time; 5) the surface can be appropriately modified with specific biomolecules (e.g. antibodies, peptides, folates, etc) to provide targeting and selectivity; 6) The luminescent properties of lanthanide-doped CP make them ideal for their using as optical nanoprobes in vivo and in vitro biological applications [10].

Nevertheless, Yb^{3+}/Tm^{3+} doped hydroxyapatite (HA) nanopowder is a weak upconversion luminescent material in the visible due to the intrinsic luminescence quenching of $^1G_4$, $^3F_2$ and $^3H_4$ excited levels of Tm^{3+} due to the optical coupling to the high frequency lattice phonons produced by the constituent OH^- free radicals (3500–2500 cm^{-1}) [13,14]. Recently, it was reported one efficient annealing process that transforms calcium deficient HA (CDHA) nanopowder into β-TCP that activated by Eu^{3+} ions exhibits an intense red luminescent emission twenty-fold higher than those obtained for europium-doped HA structure [15].

In this paper, nanocrystals of Yb/Tm:CDHA were synthesized by co-precipitation method in aqueous solution (pH adjusted to 6) and specially heat-treated with microwave at different temperatures (from 900 °C to 1000 °C) and time to produce small nanocrystals of Yb/Tm:β-TCP with less than 200 nm mean diameter of agglomerated particles and efficient UC luminescence from the $^1G_4$ (blue emission), from the $^3F_2$ (red emission) and from the $^3H_4$ (NIR emission) excited states of Tm^{3+}. This β-TCP activated by Yb^{3+} and Tm^{3+} ions constitutes a special nanophosphor with a vast biological application scope. The multiple processes of energy transfer that occurs when this material is excited around 972 nm were inspected and the UC time constants were determined. The luminescence efficiencies of $^1G_4$ and $^3F_2$ excited states (Tm^{3+}) were measured and the best treatment temperature and time under microwave heating in order to obtain a nanoparticle with an intense emission were established.

2. Experimental procedure

The nanopowders were obtained by the co-precipitation method, wherein the phosphoric acid (Synth – Brazil) diluted in deionized water (0.3 M) was slowly added drop by drop (10 mL min^{-1} rate) into a suspension of Calcium Hydroxide (Synth- Brazil), Ytterbium oxide (5.5%, Sigma Aldrich) and Thulium oxide (0.5%, Sigma Aldrich) (0.5 M). The pH values of the solutions were adjusted to 6.0 by adding HNO_3. After the precipitation, the solutions were aged at room temperature for 24 h. The precipitates were filtered and washed several times with deionized water to remove free ions. Finally, they were dried at 60 °C for 24 h.

The dried powders were heated at T=900 °C and 950 °C for 2 or 3 min, 1000 °C for 10 min using an adapted microwave oven, and at 1000 °C for 3 h using a conventional furnace. Samples were characterized by X-ray diffraction (XRD) using a Multiflex Rigaku diffractometer using the Cu kα (λ=0.1542 nm) radiation. The crystallite size was determined by Scherrer's formula and the (002) X-ray diffraction peak was used. The nanopowders were dispersed in absolute isopropanol and ultrasounds treated to avoid particles agglomeration, and then were dropped on a copper grid to be observed by transmission electronic microscopy (JEM 2010 - JEOL). To Field Emission Gun scanning electron microscopy (FEG JSM 6701F – JEOL) analysis the samples were deposited in a carbon-cement. Granulometry measurements were performed by dynamic light scattering (DLS), in a ZetaPALS-Zeta Potential Analyzer, BrookHaven Corp.

In the luminescence lifetime measurements, the samples were excited by pulsed laser radiation generated by a tunable OPO-IR pumped (Rainbow from OPOTEK, USA) by the second harmonic of a Q-switched Nd:YAG (yttrium aluminum garnet) laser (Brilliant B from Quantel, France). Laser pulse widths of 4 ns at 972 nm were used to directly excite the $^4F_{5/2}$ excited state of Yb^{3+}. Luminescence signals were analyzed by the 0.25 m Kratos monochromator, detected by the EMI S-20 PMT (response time of 10 ns) or using a charge coupled device (CCD) spectrometer coupled to the sample holder containing the nanopowder via optical fiber. Luminescence lifetime was measured using a digital oscilloscope of 100 MS s^{-1} model TDS 410 from TEKTRONIX interfaced to a microcomputer.

3. Experimental results

The as-synthesized Yb(5.5%):Tm(0.5%):CDHA nanocrystals have shown the hexagonal phase of HA ($Ca_{10}(PO_4)_6(OH)_2$) corresponding to the JCPDS file no. 9-432, with a diffraction profile broadening, as seen in Fig. 1.

The samples were calcined at temperatures higher than 900 °C in order to assess the effect of temperature versus time changes on the phase composition and formation of pure β-TCP crystal structure. It is well seen the evolution of deficient hydroxyapatite transformation into β-TCP pattern in Fig. 1. After thermal treatment at 900 °C for 2 min, the diffractogram peaks were indexed according to the standard pattern of HA and β-TCP (JCPDS 09-0169), because this short time (2 min) was not enough for the completely transformation of the powder into the rhomboidal phase. Nevertheless, after 3 min of adapted microwave heating (at 900 °C), and for all the others treatments (samples treated at 950 °C and 1000 °C), the calcined powders showed well characterized peaks of pure β-TCP diffraction pattern (Fig. 1). From the Rietveld refinement it was found out the parameter values as a=10.4300 Å and c=37.3369 Å.

The morphologies of the powders, before and after thermal treatment, are shown in Fig. 2. Despite the broadening X-Ray

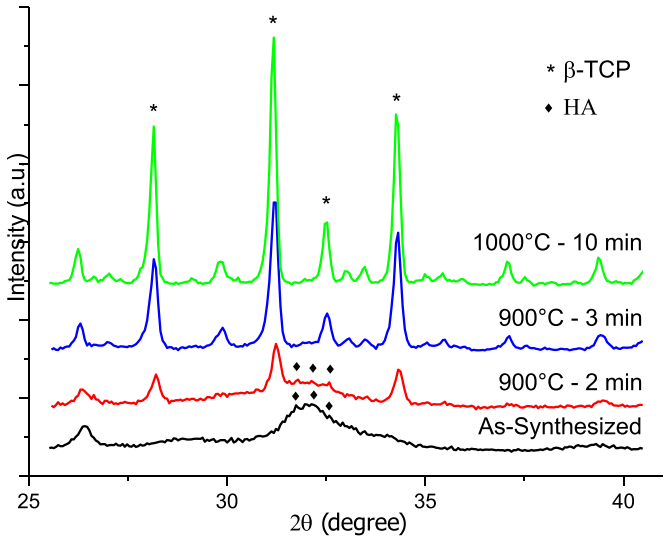

Fig. 1. X-ray diffraction pattern of Yb/Tm: β-TCP as-synthesized (HA phase), treated at 900 °C for 2 min (HA and β-TCP phases), 900 °C for 3 min (pure β-TCP phase), and at 1000 °C for 10 min (pure β-TCP phase).

diffractogram, the samples as-synthesized (the untreated Yb/Tm:CDHA) has well-defined crystalline phase (see Fig. 2(A)). Fig. 2(B) shows the sample treated at 900 °C for 2 min, Fig. 2 (C) shows those treated at 950 °C for 2 min, and Fig. 2(D) at 900 °C for 3 min.

Fig. 3 shows the samples calcined at 950 °C for 3 min (A), 1000 °C for 10 min (B) in the adapted microwave, and at 1000 °C for 3 h in a conventional furnace (C). At 1000 °C, for 10 min as for 3 h, both samples present an initial sintering and the grain growth processes, which one is even more pronounced to the sample heated at a conventional oven, for 3 h.

Particle size distribution measurements of the sample treated at 900 °C for 3 min and dispersed in water using Duramax ceramic dispersant was performed using a dynamic light scattering technique (DLS) that gave a mean particle size of 187.5 nm and exhibiting a bimodal distribution (see Fig. 4). The first peak is centered at 75 nm, and the second one is somewhat broad, centered at 240 nm, approximately. Probably, the first peak is due to the individual particle size and the second one represents the aggregated particles. This result is corroborated by the mean crystallite size of 55.3 nm calculated using the Scherrer's formula and observed in the TEM micrographs shown in Fig. 2(D).

Regarding to the luminescence properties, Yb/Tm:β-TCP nanocrystals show an upconversion process (UCP) involving the $Yb^{3+} \rightarrow Tm^{3+}$ energy transfer to produce visible emissions from the $^1G_4$ and $^3F_2$ excited states of Tm^{3+} in the blue (478 nm) and red (647 nm) spectral range respectively, and NIR emission from the $^3H_4$ level (800 nm), under laser excitation centered in the Yb^{3+} ions absorption at 972 nm. The energy transferred from the excited absorption states of Yb^{3+} to Tm^{3+} ions follows the processes below:

1. The first energy process from the Yb^{3+} ($^2F_{5/2}$) to the Tm^{3+} excites the $^3H_6$ to $^3H_5$ state;
2. Then, the Tm^{3+} ions relax nonradiatively (ΔE_1) to the $^3F_4$ state and populate the $^3F_2$, $^3F_3$ state through a second energy transfer process from the Yb^{3+} ($^2F_{5/2}$) to the Tm^{3+} ($^3F_4$);

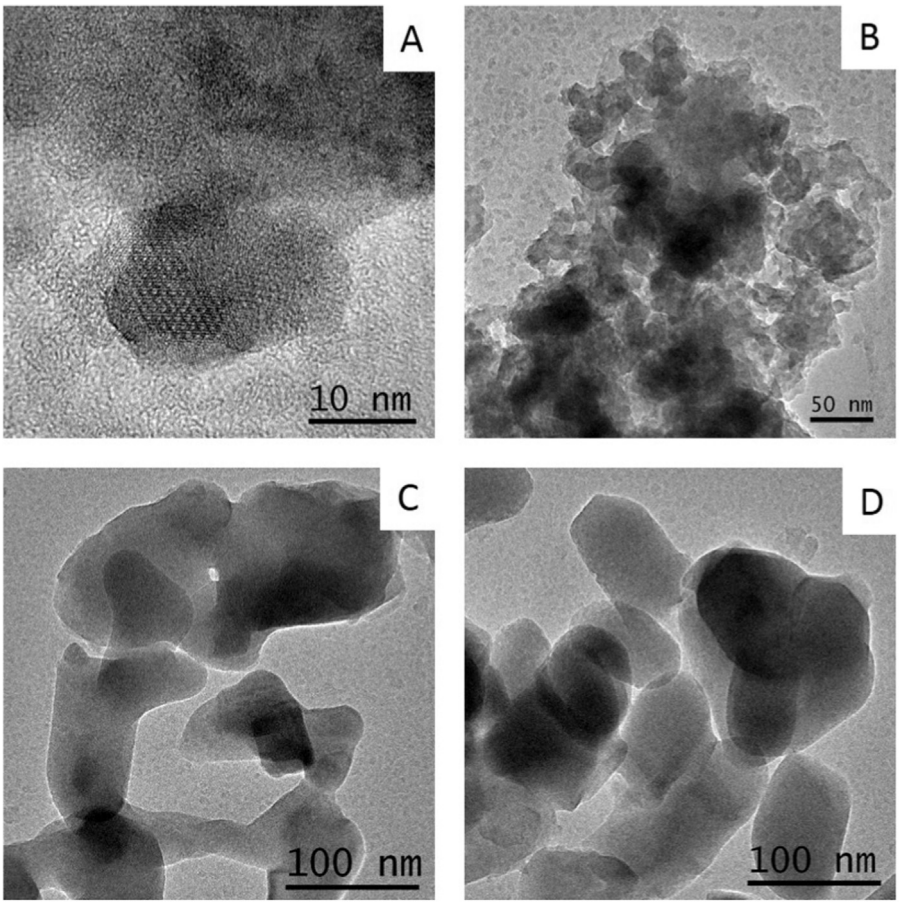

Fig. 2. TEM micrographs of the as-synthesized Yb(5.5%)Tm(0.5%):β-TCP nanopowders (A) and the samples thermally treated at T=900 °C for 2 min (B), T=950 °C for 2 min (C), and T=900 °C for 3 min (D) under an adapted microwave radiations.

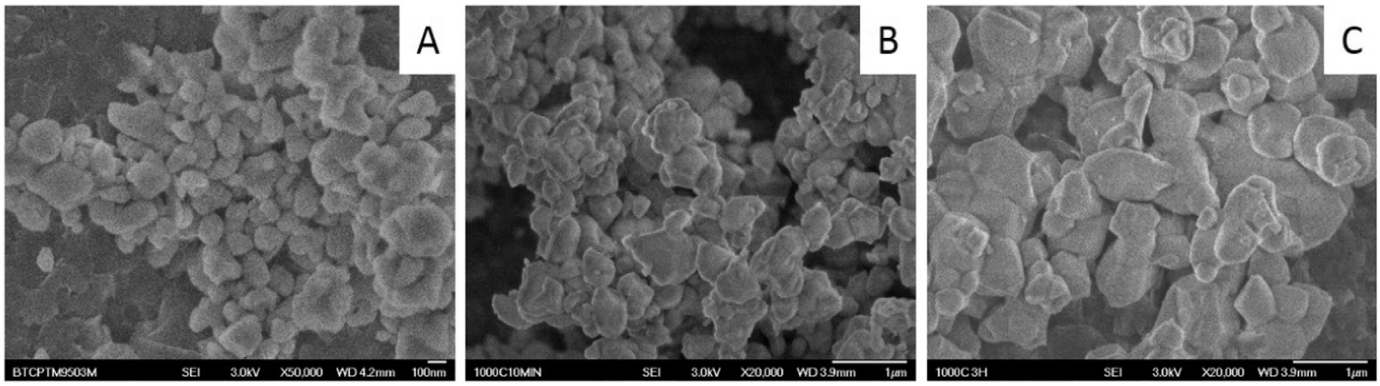

Fig. 3. FEG micrographs of the Yb(5.5%):Tm(0.5%):β-TCP nanopowders thermally treated at T=950 °C for 3 min (A) and T=1000 °C for 10 min (B) under an adapted microwave radiations, and at T=1000 °C for 3 h in a conventional furnace (C).

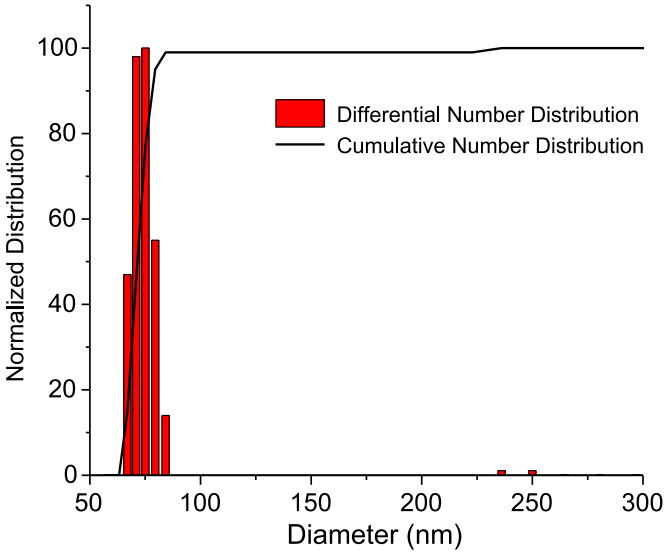

Fig. 4. Particle sizes (hydrodynamic diameter) distributions obtained with dynamic light scattering of Yb/Tm:β-TCP thermally treated at 900 °C for 3 min.

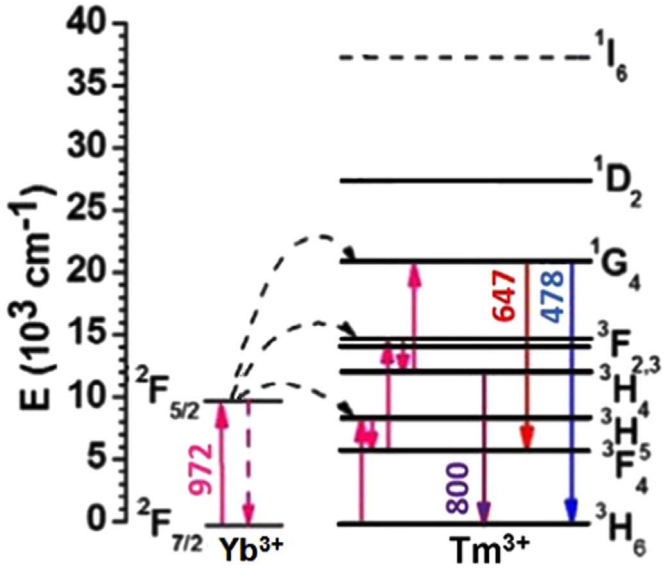

Fig. 5. Energy level diagrams of Yb^{3+} and Tm^{3+} ions, and the energy transfer mechanisms involved in the upconversion luminescence process [adapted from Ref. [16]].

3. The $^3H_4$ state is populated by the redundant energy dissipation from the $^3F_2$, $^3F_3$ state (ΔE_2), where the strong NIR can take place with peak at 800 nm arises from the Tm^{3+} ($^3H_4 \rightarrow {}^3H_6$) transition.
4. Additionally, from this Tm^{3+} ($^3H_4$) excited state a third energy transfer process occurs: from the Yb^{3+} ($^2F_{5/2}$) state to the Tm^{3+} ($^3H_4$)→Tm^{3+} ($^1G_4$) where the blue and red fluorescences are generated, which correspond to the $^1G_4 \rightarrow {}^3H_6$ (478 nm) and $^1G_4 \rightarrow {}^3F_4$ (647 nm), respectively.

Fig. 6 shows the emission spectrum of Tm^{3+} in Yb/Tm:β-TCP for nanopowders thermally treated at T=900 °C, 950 °C and 1000 °C for different times using an adapted microwave oven. The samples were excited using pulsed laser excitation with energy of 2×10^6 W cm^{-2} (E=11 mJ) at 972 nm.

The untreated sample (as-synthesized) did not exhibit fluorescence. The thermally treatment not only allows the upconversion process as it become stronger after the nanopowder treatment at higher temperature for longer time. The effects of temperature treatment on the luminescence properties have already been extensively discussed by our group [14]. Using the microwave radiation heating instead of a conventional oven, we were able to obtain intense blue, red and NIR emissions after just 3 min of calcination, at 900 °C, which is important because long thermal treatment makes the particle bigger [14].

The correlations of calcinations data (temperature versus time)

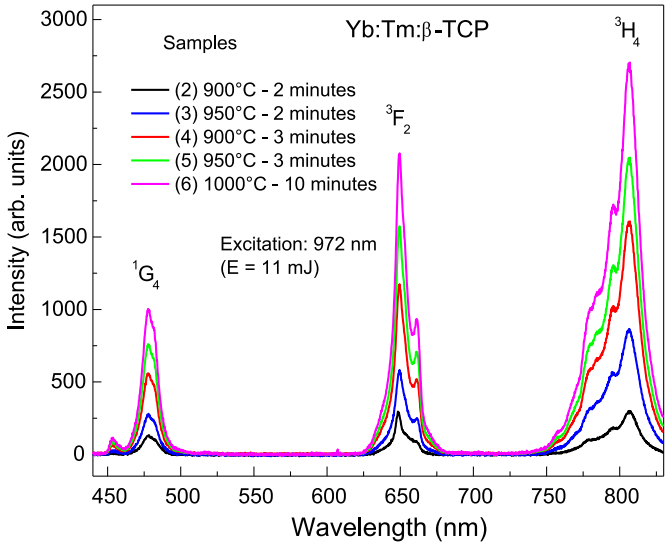

Fig. 6. Emission spectrum of Tm^{3+} excited by upconversion process in Yb(5.5%):Tm(0.5%):β-TCP nanopowder using pulsed laser with excitation energy of 2 x 10^6 W cm^{-2} (E=11 mJ) at 972 nm. It is seen an increase in intensity of visible emission of Tm^{3+} from $^1G_4$ (blue emission), $^3F_2$ (red emission) and $^3H_4$ (NIR emission) as the temperature and time thermal treatment increases.

Table 1
Samples identification, temperature, time of microwave thermal treatment and the fluorescence intensity measured for the red emission at 647 nm (arbitrary units).

Sample (#)	Temperature T (°C)	Time *t* (min)	Intensity *I* (647 nm)
(1) Yb/Tm:CDHA	as-synthesized	–	–
(2) Yb/Tm:HA - Yb/Tm: β-TCP	900	2	240
(3) Yb/Tm:β-TCP	950	2	583
(4) Yb/Tm:β-TCP	900	3	1175
(5) Yb/Tm:β-TCP	950	3	1574
(6) Yb/Tm:β-TCP	1000	10	2075

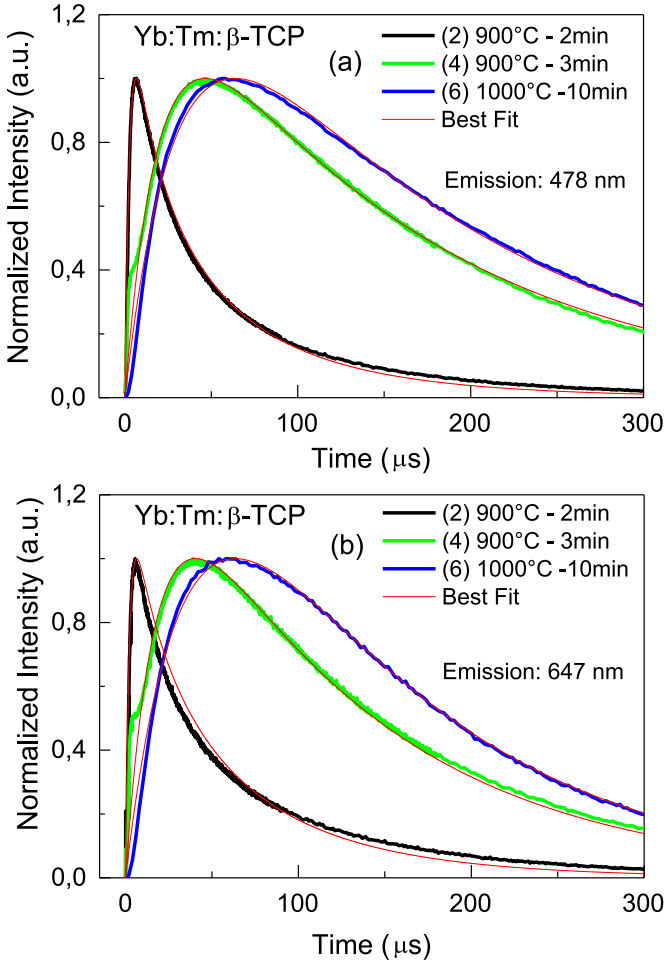

Fig. 7. Upconversion luminescence transients measured at 478 nm (a) and 647 nm (b) for Yb(5.5%)Tm(0.5%):β-TCP nanopowder thermally treated at T=900 °C for 2 and 3 min and at T=1000 °C for 10 min with a microwave oven. The emission intensities were normalized to better visualization of changes in the time-dependent signals.

and fluorescence intensity at 647 nm (red emission) are given in Table 1.

Fig. 7 shows the thermal effect produced in the upconversion luminescence transients of Tm^{3+} measured at 478 nm (a) and 647 nm (b) for Yb(5.5):Tm(0.5):β-TCP nanopowder thermally treated at T=900 °C for 2 and 3 min and at T=1000 °C for 10 min. The samples treated at 900 °C for 2 min present HA and β-TCP phases in their composition, according to DRX measurements. Nevertheless, the HA phase becomes negligible for all other heated samples. The luminescence risetime of Fig. 6 gives the upconversion time for both emissions in the blue and the red spectral region. The upconversion time becomes longer as the treatment temperature and time increase, however reaching a constant value for the treatment temperature and time equals to T=1000 °C and t=10 min or t=3 h. Similar behavior is observed for the nanopowder luminescence decays of the blue and red emission of Tm^{3+} after the microwave thermal treatments.

The luminescence transients from $^1G_4$ and $^2F_3$ excited states of Tm^{3+} were best fitted using Eq. (1), which gives phenomenological description of the $Yb^{3+} \rightarrow Tm^{3+}$ energy transfer [17].

$$I(t) = I_0[\exp(-t/t_2) - \exp(-\gamma_1\sqrt{t} - t/t_1)] \quad (1)$$

The mean value of the decay time of the $^1G_4$ or $^3F_2$ excited levels was obtained using the integration relation given by Eq. (2)

$$\tau = \int \exp(-\gamma_1\sqrt{t} - t/t_1), \quad (2)$$

where $\tau = t_1$ when γ_1 is zero. The fitting parameter t_2 is the time constant of the $Yb^{3+} \rightarrow Tm^{3+}$ upconversion process. γ_1 and t_1 are the fitting parameters used for the excited state decay. If γ_1 is equal to zero, it means that no cross-relaxation between Tm^{3+} occurs and the decay is exponential with a time constant t_1. However, if $\gamma_1 > 0$, it means that a cross-relaxation process competes with the intrinsic decay of the excited state ($^1G_4$ and $^3F_2$) and the mean lifetime of the decay is given by Eq. (2). The fitting parameters obtained from best fittings performed using the luminescence transients exhibited in Fig. 5 are given in the Tables 2 and 3.

The luminescence efficiency of $^1G_4$ (or $^3F_2$) level of Tm^{3+} was calculated using the expression given by Eq. (3)

$$E_f = \tau/\tau_d, \quad (3)$$

where τ is calculated using Eq. (2) and τ_d is the intrinsic decay of $^1G_4$ (or $^3F_2$) level. The intrinsic decay times (τ_d) of $^1G_4$ and $^3F_2$ levels were assumed to be equal to experimental decay constant (t_1) measured for the nanopowder sample treated at T=1000 °C for 10 min, which are equals to 161 μs and 122 μs, respectively.

4. Discussion

The generation of visible and NIR UC fluorescence is a multiphoton process, which can be easily obtained by the excitation with a pulsed or continuous wave NIR laser. The Tm^{3+} ions can efficiently emit photons in the blue, red and NIR regions of the spectrum and have the ability to convert IR to visible light, because the quasi-resonant energy levels of Tm^{3+} with the excited Yb^{3+} level ($^2F_{5/2}$) allows $Yb^{3+} \rightarrow Tm^{3+}$ energy transfer. It facilitates effective population inversion between the relevant energy levels $^3F_4$, $^3H_4$ and $^3H_6$ of Tm^{3+} through promoting a strong energy transfer of $Yb^{3+} \rightarrow Tm^{3+}$. The experimental results demonstrate that beta-tricalcium phosphate is a good host material for Yb^{3+} and Tm^{3+}.

Table 2
Best-fit parameters for the $^1G_4$ excited state emission transient of Tm^{3+} measured at 478 nm and luminescence efficiencies.

Best fit parameters for the $^1G_4$ level emission transient of Tm^{3+} measured at 478 nm						
Sample (#) (T and time)	t_2 (μs)	γ_1 ($s^{-1/2}$)	t_1 (μs)	τ (μs)	R^2	E_f (%)
(2) 900 °C (2 min)	2.4	188	161	32.1	0.998	20
(3) 950 °C (2 min)	23.8	64.2	161	83.7	0.997	52
(4) 900 °C (3 min)	19.7	0	153	153	0.997	95
(6) 1000 °C (10 min)	31.2	0	161	161	0.999	100

The intrinsic decay time (τ_d) of $^1G_4$ level was taken equal to the constant decay measured for the sample treated at 1000 °C for 10', i.e., $\tau_d = t_1 = 161$ μs.

Table 3
Best-fit parameters for the $^3F_2$ excited state emission transient of Tm^{3+} measured at 647 nm and luminescence efficiencies.

Best fit parameters for the $^3F_2$ level emission transient of Tm^{3+} measured at 647 nm						
Sample (#) (T and time)	t_2 (μs)	γ_1 ($s^{-1/2}$)	t_1 (μs)	τ (μs)	R^2	E_f (%)
(2) 900 °C (2 min)	2.2	136	122	39.9	0.995	33
(3) 950 °C (2 min)	29.5	35.7	122	87.2	0.999	71
(4) 900 °C (3 min)	18.1	0	120	120	0.994	98
(6) 1000 °C (10 min)	37.3	0	122	122	0.999	100

The intrinsic decay time (τ_d) of $^3F_2$ level was taken equal to the constant decay measured for the sample treated at 1000 °C for 10', i.e., $\tau_d = t_1 = 122$ μs.

The luminescence spectrum (Fig. 6) shows three UC emission bands resolved, centered at 478, 647 and 800 nm, which correspond to the $^1G_4 \rightarrow {}^3H_6$, $^1G_4 \rightarrow {}^3F_4$, and $^3H_4 \rightarrow {}^3H_6$ transitions of Tm^{3+} ions, respectively [16]. Three- and two-photon processes are involved to populate the $^1G_4$, and $^3H_4$ state, respectively [16].

The luminescence kinetics of $^1G_4$ and $^3F_2$ excited states of Tm^{3+} analyzed in the Fig. 5 shows that the risetime t_2 (or UC time) is shorter for the sample treated at T=900 °C for 2 min (t_2=2.4 μs). t_2 becomes longer as the temperature and/or time treatment increases, i. e., t_2 is equal to 37 μs for a treatment at T=900 °C for 3 min. Similar behavior is observed for the luminescence decays of $^1G_4$ and $^2F_3$ excited levels. In this case, the decay time constants of $^1G_4$ and $^3F_2$ levels increase to 153 μs and 120 μs, respectively. This effect is attributed to two distinct processes occurring during the thermal treatments: 1) CDHA crystal phase transformation into β-TCP phase, and 2) Yb^{3+} and Tm^{3+} ionic diffusions thermally activated gradually change towards a homogeneous distribution. Non-random distribution of Tm^{3+} ions in the crystal lattice propitiates the ($Tm^{3+} \times Tm^{3+}$) cross-relaxation (concentration quenching) that decreases the $^1G_4$ and $^3F_2$ excited state lifetimes and the luminescence efficiencies [18,19]. In this case, the decay is non-exponential and the energy transfer parameter γ_1 is non-zero. The results of best fitting parameters presented in Tables 2 and 3 show that γ_1 assumes large values for the initial thermal treatment at T=900 °C for 2 min. Consequently, the blue, red and NIR emissions are too weak; see the data of sample (2) in the Table 1.

The measured luminescence efficiencies of the $^1G_4$ and $^3F_2$ excited states of Tm^{3+} in Yb/Tm:β-TCP showed in Tables 2 and 3 are dependent on the temperature and time of the microwave thermal treatment, which transforms the CDHA into β-TCP crystal structure. As a consequence, the UC luminescence from Tm^{3+} increases with the temperature and time of microwave thermal treatments. This occurs because the $^1G_4$, $^3F_2$ and $^3H_4$ excited levels of Tm^{3+} that are reached by the $Yb^{3+} \rightarrow Tm^{3+}$ energy transfer (upconversion process) are strongly non-radiatively quenched in the HA (or CDHA) crystal structure [13]. This luminescence quenching of Tm^{3+} occurs due to the strong multiphonon decay induced by the high frequency (3500–2500 cm^{-1}) phonons of OH^- free radicals present in the HA crystal lattice. On the other hand, the CDHA→β-TCP phase transformation may increase the visible and NIR upconversion luminescence of Tm^{3+} as the thermal treatment becomes more effective.

We would like to highlight that the same luminescence intensity was obtained for both samples treated at 1000 °C, for 10 min with the microwave oven and for those calcined in a conventional furnace for longer time (3 h). Microwave treatment process has gained much attention recently, due the fast heating, enhanced densification rate, improved microstructure and the energy, time and cost savings when compared with conventional sintering [20]. The microwave radiation suppresses grain growth, which is attributed to the shorter calcination time and a more effective phase transformation process during microwave treatment. It was mandatory to obtain the beta-tricalcium phosphate nanoparticles sized smaller than 100 nm, emitting efficiently at 478 nm (blue), 647 nm (red) and 800 nm (NIR), produced in this work.

The NIR luminescence emission at 800 nm (and the excitation wavelength at 972 nm) are still within the spectral range of the considered "window of optical transparency" for biological tissues, allowing high contrast in vitro and in vivo optical bioimaging, as both light attenuation and scattering are significantly reduced in the NIR spectral range [21,22].

Which concerns to photodynamic therapies, most variety of PS compounds are all characterized by an intense absorption band between 400 and 430 nm (Soret Band) and weaker absorption bands (Q-bands) above 550 nm [23]. However, the penetration depth of light at Soret Bands (blue range) wavelengths in tissue is minimal. Conventionally, a laser emitting at 630 nm is used for photodynamic therapy, since Q-bands above 600 nm are normally targeted for PDT purposes; because they retain high quantum yields for PS reactions and at the same time light above 600 nm penetrates deeper into the tissue. For this reason, the increase of light penetration is considered to be an important factor in increasing the clinical efficacy of PDT [23,24]. The using of an efficient upconversion nanoparticle in conjunction with a photosensitizer could be a novel approach for PDT using infrared laser light excitation. In this approach, the efficient Yb/Tm:β-TCP nanoparticle could be excited by NIR laser and then the excitation energy transferred to a photosensitizer may occur. The PS, in proximity to the lanthanide doped-phosphate calcium (covalently bonded to it, through adsorption process), would be excited to the singlet state to produce the singlet oxygen requires to PDT [24].

Calcium phosphate nanoparticles have been proven to be an interesting class of inorganic matrices for effective delivery of targeted drugs (i.e. PS) or genes [3]. Due to their similarity to the mineral in mammals bone and teeth, low immune response and high biocompatibility, many efforts have reported calcium phosphate for non-toxic and efficient transport of bioactive agents [3].

Combined with the similarity to the mineral in human bone and teeth, excellent biocompatibility, low immune response and facile resorbability of calcium phosphates, the enhanced photophysical and optical properties make the new Yb^{3+}/Tm^{3+} doped-β-TCP a promising nanofluoroprobe for a large number of applications in the future, including biological issues.

5. Conclusions

Yb^{3+}/Tm^{3+}:β-TCP nanocrystals have been successfully synthesized by a co-precipitation method followed by a subsequent heating treatment using an adapted microwave oven. Powder X-ray diffraction, transmission and scanning electron microscopy, dynamic light scattering, upconversion photoluminescence spectra, and kinetic decay were used to characterize the samples. Under Nd:YAG laser excitation of 972 nm, the bright blue, red and NIR emissions of Yb^{3+}/Tm^{3+}:β-TCP nanocrystals at 478 nm, 647 nm and 800 nm corresponding to the $^1G_4 \rightarrow {}^3H_6$, $^1G_4 \rightarrow {}^3F_4$ and $^3H_4 \rightarrow {}^3H_6$ transitions of Tm^{3+}, respectively, were analyzed.

The experimental results of luminescence and TEM micrographs analysis have indicated that the best temperature and time to obtain a doped beta-calcium phosphate nanometric and efficient emitter was at 900 °C for 3 min using the microwave radiation. This thermal treatment can produce nanopowder constituting an ellipsoidal form with a mean crystallite size of 55.3 nm. Additionally, the measured luminescence efficiency of the blue and the red emissions were 95% and 98% relative to the

emission decays measured for the sample treated at T = 1000 °C for 10 min (or for 3 h in a conventional oven), whose luminescence efficiency was taken as 100%.

This new nano-fluoroprobe, capable of converting NIR photons to higher energy photons constitutes a promising NIR-to-Visible/NIR upconversion probes (allowing the excitation and emission to fall in the so-called "optical windows"). Although much remains to be done to effectively detect the real gains brought by this novel nanoparticles, we strongly believe that this Yb/Tm: β-TCP nanocrystals may be used as diagnostic and therapeutic agents in the future, resulting in an important strategy to help overcome certain challenges and allow them to be successfully translated into clinical use, treating and monitoring the stage of the disease using a single all-in-one particle, improving the quality of the luminescence biomedical imaging, labeling and therapy.

Acknowledgment

The authors are thankful to Dolores R. R. Lazar and Valter Ussui for their assistance with lanthanide oxides during the synthesis procedures, the Rheological Laboratory from IPEN for the DLS analysis and the Brazilian funding agency CNPq (480892/2013-0) for part of the financial support.

The authors have declared that no competing interest exists.

References

[1] A.L.B. Barros, D.C.F. Soares, Nanoparticles: imaging and therapy combined, J. Mol. Pharm. Org. Process. Res. (2014) 2–e113.
[2] S. Santra, D. Dutta, G. Walter, B. Moudgil, Fluorescent nanoparticle probes for cancer imaging, Technol. Cancer Res. Treat. 4 (2005) 6.
[3] X. He, K. Wang, Z. Cheng, In vivo near-infrared fluorescence imaging of cancer with nanoparticles-based probes, Nanomed. Nanobiotechnol. 2 (2010) 349–366.
[4] P.D. Sima, J.R. Kanofsky, Cyanine dyes as protectors of K562 cells from photosensitized cell damage, Photochem. Photobiol. 71 (2000) 413–421.
[5] G. Luker, K. Luker, Optical imaging: current applications and future directions, J. Nucl. Med. 49 (2008) 1–4.
[6] H. Zheng, D. Gao, X. Zhang, E. He, J. Appl. Phys. 104 (1) (2008) 013506.
[7] Z. Chen, H. Chen, H. HU, M. Yu, F. Li, Q. Zhang, Z. Zhou, T. Yi, C. Huang, J. Am. Chem. Soc. 130 (10) (2008) 3023.
[8] J. Zhou, F. Li, Chem. Soc. Ver. 41 (2012) 1323.
[9] C. Wang, L. Cheng, Z. Liu Z, Nanoparticles for photodynamic therapy and other therapeutics, Theranostic 3 (5) (2013) 317–330 (and references therein).
[10] C.J. Carling, F. Nourmohammadian, J.C. Boyer, N.R. Branda, Remote-control photorelease of caged compounds using near-infrared light and upconverting nanoparticles, Angew. Chem. Int. Ed. 49 (2010) 3782–3785.
[11] M.K.G. Jayakumar, N.M. Idris, Y. Zhang, Remote activation of biomolecules in deep tissues using near-infrared-to-UV upconversion nanotransducers, Proc. Natl. Acad. Sci. 109 (22) (2012) 8483–8488.
[12] H.S. Muddana, T.T. Morgan, J.H. Adair, P.J. Butler, Photophysics of Cy3-encapsulated calcium phosphate nanoparticles, Nanoletter 9 (4) (2009) 1559–1566.
[13] S. Kareiva, V. Klimavicius, A. Momot, J. Kausteklis, A. Prochodko, L. Dagys, F. Ivanauskas, S. Sakirzanovas, V. Balevicius, A. Kareiva, J. Mol. Struct. 1119 (2016) 1–11.
[14] F.R.O. Silva, N.B. Lima, L.C. Courrol, A.H.A. Bressiani, L. Gomes, Synthesis, characterization and luminescence properties of Eu^{3+}-doped hydroxyapatite nanocrystal and the thermal treatment effects, Opt. Mater. 47 (2015) 135–142.
[15] F.R.O. Silva, N.B. Lima, S.N. Guilhen, L.C. Courrol, A.H.A. Bressiani, Evaluation of europium-doped HA/BTCP ratio fluorescence in biphasic calcium phosphate nanocomposites controlled by the pH value during the synthesis, J. Lumin. 180 (2016) 177–182.
[16] H. Qiu, C. Yang, W. Shao, J. Damasco, X. Wang, H. Agren, P.N. Prasad, G. Chen, Enhanced upconversion luminescence in Yb^{3+}/Tm^{3+}-codoped fluoride active core/active shell/inert shell nanoparticles through directed energy migration, Nanomaterials 4 (1) (2014) 55–68.
[17] L.D. Da Vila, L. Gomes, L.V.G. Tarelho, J. Appl. Phys. 93 (7) (2003) 3873.
[18] Z. Chen, H. Chen, H. HU, M. Yu, F. Li, Q. Zhang, Z. Zhou, T. Yi, C. Huang, J. Am. Chem. Soc. 130 (10) (2008) 3023.
[19] J. Zhou, F. Li, Chem. Soc. Ver. 41 (2012) 1323.
[20] A. Harabi, D. Belamri, N. Karboua, F.Z. Mezahi, Sintering of bioceramics using a modified domestic microwave oven, J. Therm. Anal. Calorim. 104 (2011) 383–388 (and references therein).
[21] G. Chen, T.Y. Ohulchanskyy, R. Kumar, H. Agren, P.N. Prasad, Ultrasmall monodisperse NaYF4:Yb^{3+}/Tm^{3+} nanocrystals with enhanced near-infrared to near-infrared upconversion photoluminescence, ACS Nano 4 (6) (2010) 3163–3168.
[22] Z. Song, Y.G. Anissimov, J. Zhao, A.V. Nechaev, A. Nadort, D. Jin, T.W. Prow, M. S. Roberts, A.V. Zvygin, Background free imaging of upconversion nanoparticle distribution in human skin, J. Biomed. Opt. 18 (6) (2013) 061215.
[23] L. Brancaleon, H. Moseley, Laser and non-laser light sources for photodynamic therapy, Lasers Med. Sci. 17 (2002) 173–186.
[24] J.D. Bhawalkar, N.D. Kumar, C.F. Zhao, P.N. Prasad, Two-photon photodynamic therapy, J. Clin. Laser Med. Surg. 15 (5) (1997) 201–204.